Letter

Noise-shaped synchrony in neuronal oscillator networks

Max Contreras [*] and Philipp Hövel [†]

Theoretical Physics and Center for Biophysics, Saarland University, Campus E2 6, 66123 Saarbrücken, Germany

(Received 5 December 2025; accepted 10 July 2026; published 26 August 2026)

Stochastic fluctuations often act as promoters of activity in excitable and oscillatory systems, giving rise to phenomena such as coherence resonance. Here, we show that in the low-intensity regime, noise plays a dual role in weakly coupled neuronal units: It can both inhibit collective spiking and, with increasing intensity, restore coordinated activity. For a ring of diffusively coupled, oscillatory FitzHugh-Nagumo neurons, we demonstrate how the interplay of noise and coupling strength organizes a rich set of collective dynamical states. We systematically classify emergent dynamical scenarios by an in-depth time-series analysis that integrates multiple complementary measures. We are able to automatically identify five distinct dynamical clusters in parameter space: pure noise, quiescent state, noisy synchronization, complete synchronization, and intermittent switching. Our workflow provides a general, automated framework for characterizing collective dynamics in coupled oscillator networks.

DOI: 10.1103/sxl4-6mdm

Can complex networks benefit from noise? Although long considered detrimental [1,2], noise can shape transitions and states in complex systems, inducing synchronization [3–8], switching states [9,10], stabilizing chimera states [11,12], or creating new types of scaling behavior [13]. Recent studies also show computational advantages in learning speed [14] and even improved neural temporal coding [15] by adding random input noise. These results suggest that noise does not merely perturb complex-systems states but can fundamentally control their stability, lifetime, and transitions, enabling network-state tuning [16,17], increased efficiency [18], adaptation [19], and sensitivity [20] to external inputs.

In previous works, the impact of random perturbations [21] and different noise levels on a single oscillatory FitzHugh-Nagumo (FHN) unit has been studied [22–24] and a nonmonotone dependence of the mean spiking rate on the noise intensity has been reported. At intermediate noise levels, the spiking rate reaches a minimum, contrary to coherence resonance phenomena [25,26] observed in excitable equilibrium states.

In Ref. [24], the authors extend the classical concept of excitability (typically defined for equilibrium states) to periodic orbits: Nonlinear thresholdlike responses occur only when perturbations are applied at specific phases of the oscillation. They argue that the nonmonotone behavior can be explained by two competing effects of (i) excitation efficiency and (ii) degradation of the nonlinear response. At low noise levels, perturbations effectively trigger additional subthreshold oscillations, increasing the interval between spikes. At higher noise levels, stochastic fluctuations disrupt the deterministic structure of the system, reducing the ability of noise to induce subthreshold oscillations. This leads to an increase in the mean spiking rate again. This effect is similar to inverse stochastic resonance (ISR) [27,28], where noise paradoxically reduces the spiking frequency in neuronal systems. However, unlike ISR, which often relies on bistability, the effect arises purely from the multiscale structure of relaxation oscillations and their phase-sensitive excitability.

In a recent article [29], we studied the formation of neuronal avalanches in a ring network of diffusively coupled FHN units without noise. We found that weak coupling modifies network activity by creating distinctive intervals of spiking activity [30]. Surprisingly, increasing coupling strength does not necessarily imply more spikes, but can also lead to inhibition of activity in the network: isolated sparse spikes with intermittent bursts of synchronized neuronal firing. These mixed-mode oscillations (MMO) show that coupling can locally create subthreshold oscillations, inhibiting large avalanches in the network [31]. At the unit level, the interaction with other neurons creates small deviations in the local vector field that, close to the canard transition, can *push or pull* units from the stable orbit. Interestingly, these states show increased sensitivity and a slowdown response to external perturbations.

In this Letter, we investigate the role of small stochastic fluctuations in the emergence of distinct dynamical regimes in a coupled neuronal network. This advances our understanding of how noise can not only promote, but also inhibit collective spiking activity.

Model and methods. We consider a periodic array of N identical FHN units with nonlocal diffusive interaction. Each unit is coupled to P neighbors on either side on a one-dimensional ring [29]. There is no cross-coupling between the

[*]Contact author: mecontrl@gmx.de
[†]Contact author: philipp.hoevel@uni-saarland.de

fast (u) and slow (v) variables:

$$\epsilon \dot{u}_i = u_i - \frac{u_i^3}{3} - v_i + \frac{C}{2P} \sum_{j=i-P}^{i+P} (u_j - u_i),$$

$$\dot{v}_i = \underbrace{u_i + \alpha}_{\text{internal dynamics}} + \underbrace{\frac{C}{2P} \sum_{j=i-P}^{i+P} (v_j - v_i)}_{\text{coupling}} + \underbrace{D\,\xi_i}_{\text{noise}}. \qquad (1)$$

We scan the coupling strength C and the noise intensity D over the ranges $C \in [0, 0.1]$ and $D \in [0, 0.5]$. In Eqs. (1), ξ_i is a Gaussian white noise that independently drives the slow variable of each unit i. Throughout the Letter, we use the following parameters: $N = 50$, $P = 10$, $\epsilon = 0.05$, and $\alpha = 0.99$, that is, the uncoupled and unperturbed units operate in the oscillatory regime. We consider fixed, but random initial conditions $(u_0, v_0) \in [-2, 2]^{2N}$ and discard an initial transient of 5×10^3 time steps. For numerical integration, we use the Cash-Karp (4,5) method with adaptive step size implemented on GSL that also includes a Gaussian white noise routine to generate ξ_i [32].

For $\epsilon = 0$, a canard can be defined as the trajectory that follows the unstable branch of the critical manifold, before jumping to the left (subthreshold) or to the right (suprathreshold) stable branch [33]. For $\epsilon > 0$, one can find a ghost separatrix as introduced in Ref. [34]. Whenever a unit gets close to the escaping point following the unstable branch, at the point where the potential is minimized, noise can propel the unit to the other side, follow the canard, and then escape to the attracting branch [35]. Hence, the interplay between noise and coupling creates new, complex collective dynamics. Two exemplary cases are shown in Figs. 1(a) and 1(b) for parameter choices $(D, C) = (0.006, 0.06)$ and $(0.014, 0.06)$, respectively. The insets display the fast variable u for all N units as a space-time plot in color code. The main panels depict two snapshots of the phase space, at t_0 (blue dots) and t_1 (green dots). Highlighted in red is the unit marked by the rectangle in the respective inset (see videos in the Supplemental Material [36]). In Fig. 1(a), the network switches from quiescence to synchronization and later returns to quiescence (not shown). In quiescent periods, activity is limited to a few isolated, synchronized spiking events in small groups of units, which we call *assemblies*. Such a transition repeatedly occurs in a specific (D, C) region, close to quiescence and above a minimal coupling, as will be detailed below (see orange region in Fig. 2). Figure 1(b) depicts a noisy synchronization (NS) state with patches of synchrony and renegade nodes. The former are extended periods of spiking of the entire network with little jitter due to noise. The latter refer to a few nodes that perform differently from the rest, e.g., quiescence around t_1 while the majority of the nodes exhibit spiking. Such noisy synchronized states appear between complete synchronization (CS) and pure noise (PN, see green region in Fig. 2).

The emergence of spikes in the network results from the combined action of noise, coupling, and intrinsic dynamics. The respective vector field contributions are highlighted by green, pink, and purple normalized arrows, respectively. Remarkably, the unit close to the fixed point—red dots at times t_0 in Fig. 1(a) and t_1 in Fig. 1(b)—will not spike. The interplay

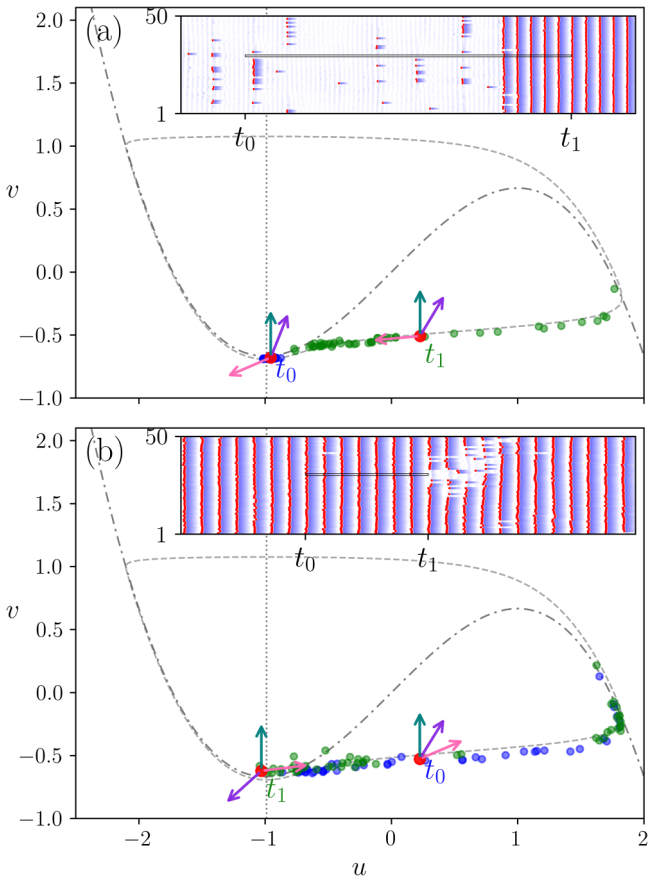

FIG. 1. Snapshots of all nodes [(u, v), main panels] at two instances, t_0 (blue dots) and t_1 (green dots), with one unit highlighted in red and space-time plots (u vs t with the location of the red node marked by a black box, insets) for (a) intermittent switching ($D = 0.006$, $C = 0.06$) and (b) noisy synchronization ($D = 0.014$, $C = 0.06$). Arrows: normalized contributions to the local vector field by noise (green), coupling (pink), and intrinsic dynamics (purple). Dash-dotted, cubic u-nullcline; dotted, vertical v-nullcline; dashed, uncoupled, unperturbed limit cycle. Corresponding videos are available in the Supplemental Material [36].

between coupling and noise on top of the intrinsic dynamics prevents a large excursion in phase space. In Fig. 1(a), this keeps the network in a quiescent state (QS), while in Fig. 1(b) it hinders collective spiking, producing small neuronal ensembles of renegade silent nodes. This yields an intermittent coexistence of local desynchronization and global synchrony within a single regime. Such a mixture of various dynamics makes it difficult to study the effect of noise in isolation. The mechanism that generates the different dynamical states is an extension of the canard- or ghost-separatrix framework developed for single units [33–35]. The push-pull effect close to the ghost separatrix is mediated through coupling with the neighbor units [29]. While coupling moves the threshold, noise will make units cross it, at a specific point on the optimal path [24,35]. In particular, in Ref. [24], perturbations applied to a single FitzHugh-Nagumo unit in the oscillatory regime trigger a nonlinear response—an extra subthreshold loop around the unstable equilibrium—only when applied during the trajectory passage near the maximum canard, verifying the results

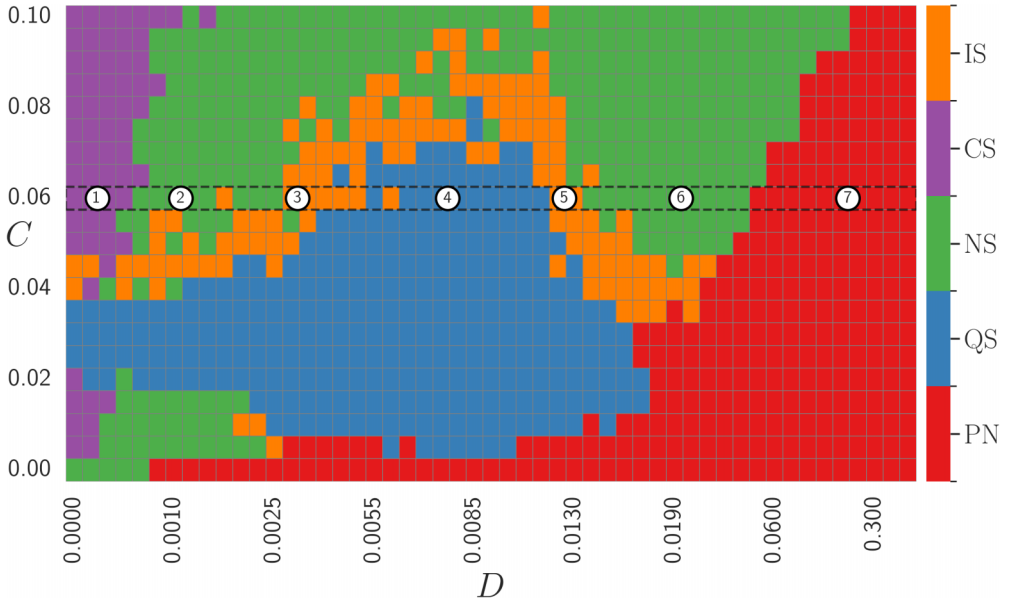

FIG. 2. Five clusters of dynamical states in the (D, C) space: red, pure noise (PN); blue, quiescent state (QS); green, noisy synchronization (NS); purple, complete synchronization (CS); orange, intermittent switching (IS). Dashed: coupling strength $C = 0.06$ used in Figs. 1, 3, and 4.

obtained in Ref. [34]. To investigate the interplay of coupling and noise, we propose a framework for identifying and grouping different collective states in the following.

To characterize dynamical states, we extract spike events directly from the time series u_i for a given combination (D, C) via a peak-detection algorithm that leads to a spike train for each unit $i = 1, \ldots, N$. Spike events are identified as local maxima that exceed a fixed threshold and are separated by a minimum temporal distance, using a peak-finding routine [37]. To classify the dynamical states throughout the entire (D, C) space, we design and apply a four-step data analysis pipeline: (i) *metrics*, (ii) *correlations*, (iii) *principal components*, and (iv) *clustering*.

The first step is to analyze the spike-train data via a comprehensive set of 12 complementary metrics that together capture individual spiking properties as well as collective network dynamics: The level of activity (mean firing rate ν), the variability of activity (Fano factor ψ and global and local coefficients of variation CV and CV_2), the collective structure (size Λ and size variability σ of assemblies and their respective connected metrics Γ_Λ and Γ_σ), the temporal coordination (spike contrast κ and spike synchronization ζ), and the dissimilarity [spike distance λ and interspike interval (ISI) distance ω]. All metrics are available in the ELEPHANT toolbox [38] and in the PYSPIKE library [39], with the exception being the connected-assemblies metrics (Γ_Λ, Γ_σ) that were self-developed on the basis of a depth-first search algorithm. They calculate the size of spiking subgraphs, providing two outputs: the size of the largest connected assembly and their variability. This contrasts with complexity (Λ, σ) that counts the number of spikes, i.e., nonempty bins, across spike trains. The result is a set of metric values for each point in (D, C). Note that the set of considered measures can be extended, making the proposed framework very versatile.

To exclude near-duplicate pairs with high correlation, the second step filters redundant metrics and selects only measures that help differentiate between dynamical states and make the difference in the observed regimes interpretable. We compute linear (Pearson) and nonlinear (Spearman and Kendall) correlation matrices to reduce to a core subset of metrics. In our case, we drop CV_2, Γ_σ, ζ, and λ and thus identify a set of eight metrics that quantify different properties of the dynamics.

The third step applies a principal component analysis [40] that serves two critical purposes: First, it eliminates any residual multicollinearity not removed by the pairwise analysis. Second, retaining only the leading components that capture most of the variance creates a low-dimensional representation. We retain the first three principal components that capture 91.9% of the cumulative variance—above the conventional 80% threshold.

For the fourth and final step, we identify clusters in the space spanned by the computed principal components. For this purpose, we employ a k-means algorithm [41] with k-means++ initialization [42], running multiple random restarts and several independent seeds. For every k, i.e., the number of clusters, we calculate two quality scores: silhouette score Q_S and Davies-Bouldin index Q_{DB} [43–46]. Table I summarizes the clustering scores for $k \in \{3, \ldots, 7\}$. Higher

TABLE I. Silhouette score Q_S and Davies-Bouldin index Q_{DB} in dependence on the number of clusters k for three principal components. Bold: highest/lowest values of Q_S/Q_{DB}.

k	3	4	5	6	7
Q_S	0.565	0.614	**0.663**	0.651	0.614
Q_{DB}	0.856	0.564	**0.549**	0.619	0.598

and lower values for Q_S and Q_{DB} correspond to stronger consistency in the clustering. Hence, we find $k = 5$ as the optimal value. These five clusters differ systematically in firing-rate variability, spike-time regularity, and population synchrony. This final step in our data analysis pipeline automatically selects the number of clusters that best captures the underlying structure of the multidimensional feature space given by the considered measures. k means is well suited to this exploratory context because the dynamical states are not known *a priori* and the data carry no labels. We explicitly handle the limitations of this method using the k-means $++$ initialization (sensitivity to centroid placement) and using different k values with scores (k must be given in advance) [47–49]. The results can be validated using raster or space-time plots as well as phase-space trajectories both at the unit and network level to confirm that each calculated cluster indeed classifies a different network dynamical state.

Results and discussion. The spiking activity of the FHN ring network without noise was described and analyzed in Ref. [29]. In short, increasing the coupling strength can drive the network from CS into QS with sparse spiking activity. Synchronization is restored at higher coupling strengths, yielding a small parameter range for *coupling-induced inhibition*.

This effect is included in Fig. 2 for $D = 0$, where increasing C first suppresses activity and generates QS states ($C \approx 0.03$, blue region), and then drives the network back into the CS regime ($C \geqslant 0.05$, purple region), where units spike synchronously. QS states give rise to a baylike domain in the (D, C) plane that for increasing noise intensity D widens at first and then narrows again until it vanishes around $D \approx 0.017$. In this regime, activity displays very low firing rates, pronounced variability, and long interspike intervals, with only sporadic recruitment of small assemblies.

Figure 2 also shows the regions of three additional clusters, out of the five identified via the data analysis pipeline described above. PN states (red region) show no assembly structure with units firing frequently and independently in an overall fast asynchronous regime. They are located in the high-noise and low-coupling areas. In noisy synchronization (green regions), we observe states close to coherence with jitters around a CS state [see inset of Fig. 1(b)]. These states exist mainly between CS and PN areas. Finally, in the intermittent-switching regime (IS, orange regions), the dynamics alternate between noisy synchronized activity and episodes of either quiescence or avalanches [see inset of Fig. 1(a)]. These special states exist almost exclusively around the top part of the QS region as a self-sustained switching phase.

As a key point of the present Letter, our results indicate the existence of noise-induced inhibition and activation transitions in the FHN network. To illustrate this, we have highlighted $C = 0.06$ in Fig. 2. We then follow the changes in dynamical states as noise increases, from left to right. Starting from CS (1), increasing noise can pull a few units—momentarily or for a few cycles—out of full synchrony, creating NS (2) through jitters and renegade nodes. Nevertheless, the system remains mainly synchronized. Further increase in D leads to IS (3), where assemblies push and pull other units, generating self-sustained extended MMO characterized by switching between collective behaviors. Intermediate D levels break down large assemblies and increase the interspike interval, putting the network in QS (4).

Paradoxically, more noise creates collective spiking patterns in an IS state (5), with assemblies and avalanches. Random perturbations push a few units away from the fixed point and activate other units via coupling. The closeness to the maximum canard trajectory [22,50,51] amplifies any momentary, noise-aligned coordination, as in ISR, while phase-sensitive excitability [24] makes units more likely to respond coherently when a connected neighbor spikes. This phenomenon becomes even more dominant with larger noise, generating a second phase of NS (6). Finally, higher noise disrupts the nonlinear response, creating a PN region (7).

Next, we characterize these regimes in more detail by examining how their temporal and spatial structure changes with noise. In particular, we consider the same horizontal cut for a fixed coupling strength $C = 0.06$ and focus on four metrics: spike contrast κ [52] and autocorrelation ρ (Fig. 3), interspike interval distance ω, and power spectral density (PSD) (Fig. 4). This links each cluster to a distinct dynamical state and measures the inhibition or activation transitions. The results show that each regime leaves a distinct signature across assembly size, variability, and synchrony.

In the CS state [insets (a) of Figs. 3 and 4], all units spike together at a specific frequency and with a periodic autocorrelation function. The firing rate matches that of an isolated unit, with no variability ($\psi, \mathrm{CV} \to 0$) but perfect synchrony ($\kappa = 1$) and zero ISI distance ($\omega = 0$), and the avalanches span the entire network ($\Gamma_\Lambda = \Lambda = N$).

In both NS bands [insets (b) and (c) of Figs. 3 and 4], the network maintains the CS firing rate but loses strict phase coherence, developing jitters and occasional renegade units [see Fig. 1(b)]. The similarity metrics decrease from their maximum CS values ($\kappa < 1$), and the dissimilarity increases ($\omega > 0$). We find a slowly decaying ρ, while the PSD still shows a pronounced but widened peak above a noise floor. The low-noise NS band remains close to CS, with relatively high κ and small ω and almost no renegade nodes. In contrast, the high-noise NS band exhibits renegades reducing similarity ($\kappa \approx 0.9$), with almost the same firing rate and variability, and an increased dissimilarity ($\omega \approx 0.1$), revealing a more strongly noise-perturbed collective oscillation. This is reflected in the inset Fig. 3(c), where ρ decays much faster than in (b). Similarly, the inset Fig. 4(c) depicts lower peaks compared to background noise, which are shifted from the free-running frequency.

The IS states are characterized by alternating periods of noisy, avalanchelike activity and quiescent intervals, during which assemblies repeatedly form and fragment. Transitions occur in both directions: quiescent phases may evolve into noisy synchronous episodes, with or without renegade nodes, and these episodes may subsequently break into smaller assemblies or return to silence. An example of such a transition is shown in Fig. 1(a). In terms of metrics, the IS states occupy intermediate values between CS and QS. This mixed-mode switching produces highly variable synchrony, reflected in the broad range $0.4 \leqslant \kappa < 1$ (Fig. 3). Dissimilarity also indicates the mixture, $0.08 < \omega < 0.5$ (Fig. 4), resulting in peak ISI variability CV. Despite intermittent and irregular dynamics,

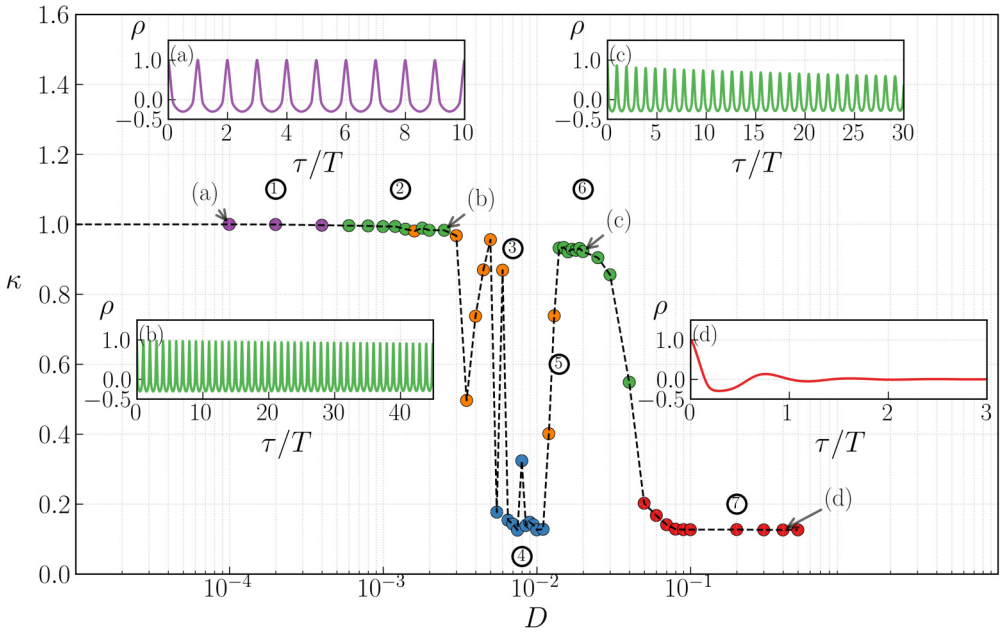

FIG. 3. Spike contrast κ and selected autocorrelation functions (insets). Colors as in Fig. 2.

the largest assembly typically remains of size N, indicating that the entire network can still participate in collective events.

In the QS regime, activity becomes sparse and weakly coordinated. Spike events appear isolated and scattered, with sporadic single-unit firing rather than collective or rhythmic bursts. The dynamics resemble the first part of the inset in Fig. 1(a). The network exhibits its highest levels of spike and ISI variability, while population activity drops ($\nu \to 0$) and pronounced avalanches disappear. In Fig. 3, κ shows a minimum value while in Fig. 4, ω peaks, indicating a highly irregular dynamical phase. These states were extensively studied in Ref. [29].

Finally, in the PN region, we observe strongly uncoordinated, burst-dominated dynamics. This corresponds to higher firing rates and lower levels of synchrony. This region extends asymmetrically with noise, starting wide with low coupling, indicating the nonlinear interplay between these two parameters [24].

Conclusions. In a weakly coupled ring of oscillatory FHN units, noise acts as a bidirectional control of collective activity: increasing its intensity first suppresses coordinated firing (inhibition, $2 \to 4$ in Fig. 2) and then restores it (activation, $4 \to 6$). This interplay of noise and coupling creates quiescent states and transitional phases—new dynamical states observed

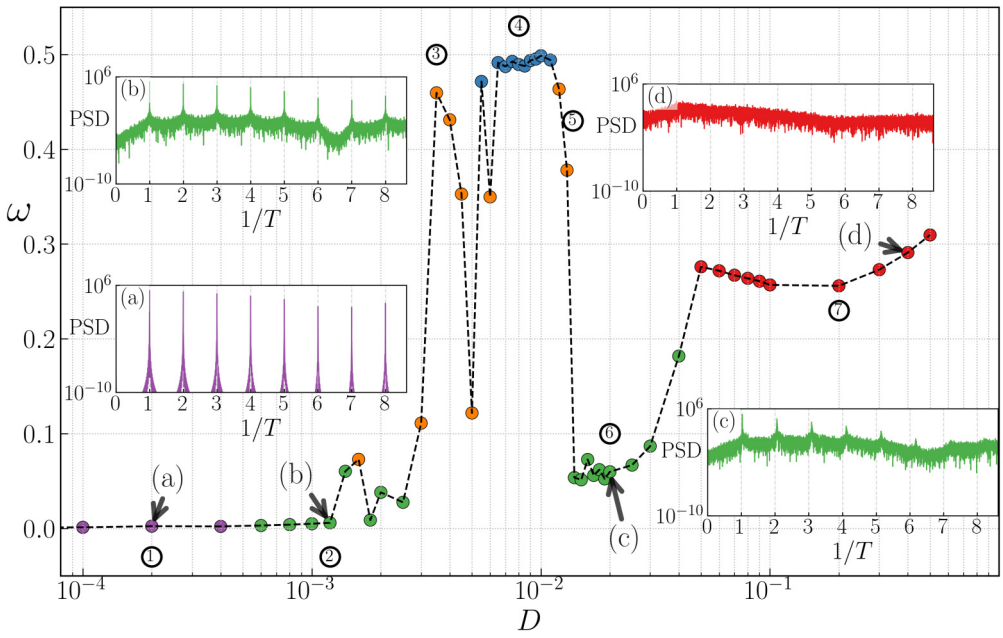

FIG. 4. Interspike interval distance ω and selected power spectral density functions (insets). Colors as in Fig. 2.

only for weak intensities. Such a paradoxical role of perturbations is not unique to noise: In conductance-based cortical network models, low-dose propofol, whose direct action is inhibitory, produces collective excitation within a narrow dose window, with normal inhibition recovered at higher doses [53]. In our model, coupling creates quiescence in oscillatory units [29], and the nonmonotone response of the mean firing rate to noise [24] amplifies this effect over a larger range of coupling strengths.

Our results have shown that inhibition or activation phenomena do not necessarily rely on bistability as for inverse stochastic resonance. Instead, they can arise from the relaxation oscillations and phase-sensitive excitability as demonstrated for neuronal units operating in their oscillatory or limit-cycle regime. This requires operating close to the Hopf transition ($|\alpha| = 1$), where the units follow canardlike orbits that remain close to the fold; only then can weak noise and coupling tip them across the ghost separatrix, so that the dual inhibition or activation effect is not expected far from this regime. Diffusive coupling can push or pull units near the canard transition changing spike timing, while noise can reinforce or hinder this effect, sometimes prolonging interspike intervals (inhibition) and sometimes promoting coordinated responses through coupling (activation). It is a geometric effect, making the absolute magnitude of each component less relevant than the relative position to the ghost separatrix. The observed transitions are therefore a network effect of both coupling and noise acting on the system's intrinsic slow-fast dynamics. This is reminiscent of stochastic or P-bifurcations, which can be quantified by changes in the stationary and transient probability density distributions [54,55]. In practical terms, this creates new states not observed in previous studies: noisy synchronization and intermittent switching. Their sensitivity to external perturbations like the input from another neuronal network, and underlying microscopic mechanisms, are interesting questions for future research. Specifically, we need to explore how the proximity to the maximum canard and the influence of different vector fields on the units can generate oscillations of varying amplitude. This understanding could guide the fine-tuning of the network's state using noise [15–17], making it more efficient [14,18] and sensitive [20,56] to external inputs. This suggests a possible analogy to the cocktail-party effect, where an intermediate level of background noise can facilitate signal discrimination. In the present context, a specific noise range may enhance the network's responsiveness to external inputs, whereas too little or too much noise may be detrimental. We emphasize that this interpretation is speculative and warrants systematic investigation, for example, by quantifying information transmission and flow within the network using semantic or information-theoretic approaches. These questions can be further explored via semantic information theory [57,58] measuring how information flows within the network [59].

Furthermore, we have developed a data analysis pipeline that combines many complementary measures of time-series analysis to identify and classify the observed dynamical states. We have approached this issue differently from the standard way that looks for the best metric carefully selected to quantify a given state. Instead, we have developed a flexible, metric-agnostic approach, letting the data decide which metrics are the most relevant to distinguish emerging dynamical states. This framework could be applied to reveal additional structures and previously hidden patterns in similar, already studied datasets in neurobiology.

Acknowledgments. P.H. acknowledges support by the Deutsche Forschungsgemeinschaft (DFG, German Research Foundation)—Project No. 434434223—SFB 1461. M.C. wishes to acknowledge Viola Priesemann and Morten Brøns for providing useful information.

Data availability. The data that support the findings of this article are openly available [60].

[1] G. B. Ermentrout, R. F. Galán, and N. N. Urban, Reliability, synchrony and noise, Trends Neurosci. **31**, 428 (2008).

[2] I. Kanitscheider, R. Coen-Cagli, and A. Pouget, Origin of information-limiting noise correlations, Proc. Natl. Acad. Sci. USA **112**, E6973 (2015).

[3] O. V. Popovych, S. Yanchuk, and P. A. Tass, Self-organized noise resistance of oscillatory neural networks with spike timing-dependent plasticity, Sci. Rep. **3**, 2926 (2013).

[4] Z. G. Nicolaou, M. Sebek, I. Z. Kiss, and A. E. Motter, Coherent dynamics enhanced by uncorrelated noise, Phys. Rev. Lett. **125**, 094101 (2020).

[5] Y. Zhang, J. L. Ocampo-Espindola, I. Z. Kiss, and A. E. Motter, Random heterogeneity outperforms design in network synchronization, Proc. Natl. Acad. Sci. USA **118**, e2024299118 (2021).

[6] I. Belykh, E. de Lange, and M. Hasler, Synchronization of bursting neurons: What matters in the network topology, Phys. Rev. Lett. **94**, 188101 (2005).

[7] S. Martineau, T. Saffold, T. T. Chang, and H. Ronellenfitsch, Enhancing synchronization by optimal correlated noise, Phys. Rev. Lett. **128**, 098301 (2022).

[8] B. R. R. Boaretto, E. E. N. Macau, and C. Masoller, Noise-induced extreme events in Hodgkin–Huxley neural networks, Chaos Solit. Fractals **194**, 116133 (2025).

[9] D. K. Wells, W. L. Kath, and A. E. Motter, Control of stochastic and induced switching in biophysical networks, Phys. Rev. X **5**, 031036 (2015).

[10] G. Ghoshal, A. P. Muñuzuri, and J. Pérez-Mercader, Emergence of a super-synchronized mobbing state in a large population of coupled chemical oscillators, Sci. Rep. **6**, 19186 (2016).

[11] Y. Zhang, Z. G. Nicolaou, J. D. Hart, R. Roy, and A. E. Motter, Critical switching in globally attractive chimeras, Phys. Rev. X **10**, 011044 (2020).

[12] Y. Zhang and A. E. Motter, Mechanism for strong chimeras, Phys. Rev. Lett. **126**, 094101 (2021).

[13] S. Olmi and A. Politi, Crisis in time-dependent dynamical systems, Phys. Rev. Lett. **134**, 147202 (2025).

[14] N. Rungratsameetaweemana, R. Kim, T. Chotibut, and T. J. Sejnowski, Random noise promotes slow heterogeneous synaptic dynamics important for robust working memory computation, Proc. Natl. Acad. Sci. USA **122**, e2316745122 (2025).

[15] M. A. Kamaleddin, A. Shifman, N. Abdollahi, D. Sigal, S. Ratté, and S. A. Prescott, Physiological noise facilitates multiplexed coding of vibrotactile-like signals in somatosensory cortex, Proc. Natl. Acad. Sci. USA **119**, e2118163119 (2022).

[16] J. H. Meng and H. Riecke, Synchronization by uncorrelated noise: Interacting rhythms in interconnected oscillator networks, Sci. Rep. **8**, 6949 (2018).

[17] H. Yamamoto, F. P. Spitzner, T. Takemuro, V. Buendía, H. Murota, C. Morante, T. Konno, S. Sato, A. Hirano-Iwata, A. Levina, V. Priesemann, M. A. Muñoz, J. Zierenberg, and J. Soriano, Modular architecture facilitates noise-driven control of synchrony in neuronal networks, Sci. Adv. **9**, eade1755 (2023).

[18] D. R. Chialvo, G. A. Cecchi, and M. O. Magnasco, Noise-induced memory in extended excitable systems, Phys. Rev. E **61**, 5654 (2000).

[19] G. Tkačik, J. S. Prentice, V. Balasubramanian, and E. Schneidman, Optimal population coding by noisy spiking neurons, Proc. Natl. Acad. Sci. USA **107**, 14419 (2010).

[20] R. K. Adair, Noise and stochastic resonance in voltage-gated ion channels, Proc. Natl. Acad. Sci. USA **100**, 12099 (2003).

[21] M. Brøns, Excitation and annihilation in the FitzHugh-Nagumo equation, IMACS Trans. Sci. Comput. **1**, 297 (1989).

[22] V. A. Makarov, V. I. Nekorkin, and M. G. Velarde, Spiking behavior in a noise-driven system combining oscillatory and excitatory properties, Phys. Rev. Lett. **86**, 3431 (2001).

[23] C. B. Muratov and E. Vanden-Eijnden, Noise-induced mixed-mode oscillations in a relaxation oscillator near the onset of a limit cycle, Chaos **18**, 015111 (2008).

[24] I. Franović, O. E. Omel'chenko, and M. Wolfrum, Phase-sensitive excitability of a limit cycle, Chaos **28**, 071105 (2018).

[25] A. N. Pisarchik and A. E. Hramov, Coherence resonance in neural networks: Theory and experiments, Phys. Rep. **1000**, 1 (2023).

[26] A. N. Pisarchik, V. A. Maksimenko, A. V. Andreev, N. S. Frolov, V. V. Makarov, M. O. Zhuravlev, A. E. Runnova, and A. E. Hramov, Coherent resonance in the distributed cortical network during sensory information processing, Sci. Rep. **9**, 18325 (2019).

[27] M. Uzuntarla, E. Barreto, and J. J. Torres, Inverse stochastic resonance in networks of spiking neurons, PLoS Comput. Biol. **13**, e1005646 (2017).

[28] M. E. Yamakou, J. Zhu, and E. A. Martens, Inverse stochastic resonance in adaptive small-world neural networks, Chaos **34**, 113119 (2024).

[29] M. Contreras, E. S. Medeiros, A. Zakharova, P. Hövel, and I. Franović, Scale-free avalanches in arrays of FitzHugh-Nagumo oscillators, Chaos **33**, 093106 (2023).

[30] R. M. D'Souza, M. di Bernardo, and Y.-Y. Liu, Controlling complex networks with complex nodes, Nat. Rev. Phys. **5**, 250 (2023).

[31] G. Mikaberidze and R. M. D'Souza, Sandpile cascades on oscillator networks: The BTW model meets Kuramoto, Chaos **32**, 053121 (2022).

[32] M. Galassi and B. Gough, *GNU Scientific Library: Reference Manual* (Network Theory Ltd., Bristol, UK, 2009).

[33] E. M. Izhikevich, *Dynamical Systems in Neuroscience: The Geometry of Excitability and Bursting*, Computational Neuroscience (MIT Press, Cambridge, MA, 2007).

[34] I. A. Khovanov, A. V. Polovinkin, D. G. Luchinsky, and P. V. E. McClintock, Noise-induced escape in an excitable system, Phys. Rev. E **87**, 032116 (2013).

[35] Z. Chen, J. Zhu, and X. Liu, Crossing the quasi-threshold manifold of a noise-driven excitable system, Proc. R. Soc. A **473**, 20170058 (2017).

[36] See Supplemental Material at http://link.aps.org/supplemental/10.1103/sxl4-6mdm for animations of the dynamics depicted in Fig. 1.

[37] P. Virtanen, R. Gommers, T. E. Oliphant, M. Haberland, T. Reddy, D. Cournapeau, E. Burovski, P. Peterson, W. Weckesser, J. Bright, S. J. van der Walt, M. Brett, J. Wilson, K. J. Millman, N. Mayorov, A. R. J. Nelson, E. Jones, R. Kern, E. Larson, C. J. Carey, *et al.*, SciPy 1.0: Fundamental algorithms for scientific computing in Python, Nat. Methods **17**, 261 (2020).

[38] M. Denker, A. Yegenoglu, and S. Grün, Collaborative HPC-enabled workflows on the HBP Collaboratory using the Elephant framework, Neuroinformatics, 2018, doi: 10.12751/incf.ni2018.0019.

[39] M. Mulansky and T. Kreuz, PySpike—A Python library for analyzing spike train synchrony, SoftwareX **5**, 183 (2016).

[40] S. Mimar and G. Ghoshal, A sampling-guided unsupervised learning method to capture percolation in complex networks, Sci. Rep. **12**, 4147 (2022).

[41] S. Lloyd, Least squares quantization in PCM, IEEE Trans. Inf. Theory **28**, 129 (1982).

[42] D. Arthur and S. Vassilvitskii, k-means++: the advantages of careful seeding, in *Proceedings of the Eighteenth Annual ACM-SIAM Symposium on Discrete Algorithms* (SIAM, Philadelphia, PA, 2007), pp. 1027–1035.

[43] P. J. Rousseeuw, Silhouettes: A graphical aid to the interpretation and validation of cluster analysis, J. Comput. Appl. Math. **20**, 53 (1987).

[44] D. L. Davies and D. W. Bouldin, A cluster separation measure IEEE Trans. Pattern Anal. Mach. Intell. **PAMI-1**, 224 (1979).

[45] C. R. Caro-Martín, J. M. Delgado-García, A. Gruart, and R. Sánchez-Campusano, Spike sorting based on shape, phase, and distribution features, and *K*-TOPS clustering with validity and error indices, Sci. Rep. **8**, 17796 (2018).

[46] A. M. Ikotun, F. Habyarimana, and A. E. Ezugwu, Benchmarking validity indices for evolutionary K-means clustering performance, Sci. Rep. **15**, 21842 (2025).

[47] *Data Clustering: Algorithms and Applications*, edited by C. C. Aggarwal and C. K. Reddy (CRC Press, Boca Raton, FL, 2014).

[48] A. A. Wani, Comprehensive analysis of clustering algorithms: Exploring limitations and innovative solutions, PeerJ Comput. Sci. **10**, e2286 (2024).

[49] M. G. H. Omran, A. P. Engelbrecht, and A. Salman, An overview of clustering methods, Intell. Data Anal. **11**, 583 (2007).

[50] M. Krupa and P. Szmolyan, Relaxation oscillation and canard explosion, J. Diff. Equ. **174**, 312 (2001).

[51] M. Wechselberger, J. Mitry, and J. Rinzel, Canard theory and excitability, in *Nonautonomous Dynamical Systems in the Life Sciences*, edited by P. E. Kloeden and C. Pötzsche, Canard Theory and Excitability (Springer, New York, 2013), pp. 89–132.

[52] M. Ciba, T. Isomura, Y. Jimbo, A. Bahmer, and C. Thielemann, Spike-contrast: A novel time scale independent and multivariate measure of spike train synchrony, J. Neurosci. Methods **293**, 136 (2018).

[53] M. M. McCarthy, E. N. Brown, and N. Kopell, Potential network mechanisms mediating electroencephalographic beta rhythm changes during propofol-induced paradoxical excitation, J. Neurosci. **28**, 13488 (2008).

[54] L. Arnold, *Random Dynamical Systems* (Springer-Verlag, Berlin, 1998).

[55] N. S. Namachchivaya, Stochastic bifurcation, Appl. Math. Comput. **38**, 101 (1990).

[56] T. Zheng, K. Kotani, and Y. Jimbo, Distinct effects of heterogeneity and noise on gamma oscillation in a model of neuronal network with different reversal potential, Sci. Rep. **11**, 12960 (2021).

[57] D. R. Sowinski, A. Frank, and G. Ghoshal, Information-theoretic description of a feedback-control Kuramoto model, Phys. Rev. Res. **6**, 043188 (2024).

[58] S. Bartlett, A. W. Eckford, M. Egbert, M. Lingam, A. Kolchinsky, A. Frank, and G. Ghoshal, Physics of life: Exploring information as a distinctive feature of living systems, PRX Life **3**, 037003 (2025).

[59] G. Mikaberidze, O. Artime, A. Díaz-Guilera, and R. M. D'Souza, Multiscale field theory for network flows, Phys. Rev. X **15**, 021044 (2025).

[60] M. Contreras and P. Hövel, Noise-shaped synchrony in neuronal oscillator networks, GitHub, 2026, https://github.com/MaxCL/Noise_shaped_synchrony_FHN_network.